

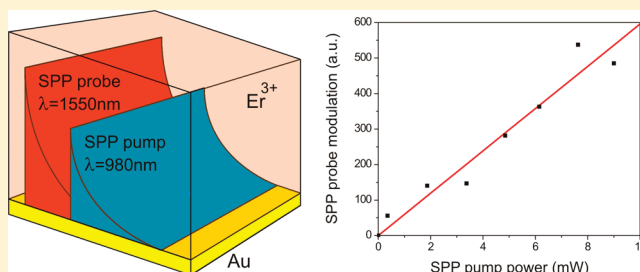
# All-Plasmonic Modulation via Stimulated Emission of Copropagating Surface Plasmon Polaritons on a Substrate with Gain

Alexey V. Krasavin,\* Thanh Phong Vo,<sup>†</sup> Wayne Dickson, Pádraig M. Bolger,<sup>‡</sup> and Anatoly V. Zayats

Nano-optics and Near-field Spectroscopy Group, Department of Physics, King's College London, Strand, London WC2R 2LS, United Kingdom

**ABSTRACT:** We experimentally demonstrate suppressed absorption and stimulated emission of surface plasmon polaritons (SPP) leading to all-plasmonic modulation of an SPP signal propagating at the interface between a metal and a gain medium; these observations are supported by the developed theory. The use of copropagating signal and control waves can provide more than 10 times more efficient SPP stimulated emission compared to out-of-plane pumping and opens up the possibility to realize integratable plasmonic components for active nanophotonic circuitry.

**KEYWORDS:** Plasmonics, plasmonic waveguides, surface plasmon polariton amplification



All-optical modulation and switching of photonic signals is a key requirement for modern photonic technologies to move toward transparent optical networks for both telecom and inter/intrachip interconnects in an attempt to cope with increasing data-rate (bandwidth) demands. All-optical devices rely on nonlinear optical interactions and thus require either high light intensities and/or a long interaction length between the signal and control light to generate a sizable effect. Recently, low power all-optical modulation has been achieved with plasmonic structures relying on the enhanced effective nonlinearities which arise due to the field confinement related to plasmonic states and their sensitivity to the refractive index of the adjacent medium, in particular close to the interface.<sup>1,2</sup> Plasmonic-based all-optical switching has been proposed and demonstrated with Kerr-type nonlinearities utilizing plasmonic crystals and localized surface plasmons (see ref 2 for recent review and references therein), absorption modulation of surface plasmon polariton (SPP) waves guided at a planar interface or in a waveguide,<sup>3–5</sup> and resonant waveguiding plasmonic devices, such as Bragg-gratings, Mach-Zehnder interferometers, and ring-resonators.<sup>6–8</sup> However, the majority of these demonstrations relied on external illumination of the plasmonic structure and are thus not suitable for integration into a complete nanophotonic circuit.

In parallel, the amplification of SPP signals has recently attracted significant attention as a means to mitigate the propagation (Ohmic) losses of plasmonic waveguides.<sup>7,9,10</sup> Several lasing materials have been used for this purpose, such as dye molecules,<sup>11–14</sup> Er<sup>3+</sup>-ions,<sup>15</sup> and semiconductor quantum dots.<sup>16,17</sup> Some of these require the constant circulation of active medium due to photobleaching, others rely on waveguides with a rather large (~10 μm) mode area, and therefore do not address the question of amplification of confined SPP waves. While various organic molecules provide higher gain values, inorganic materials are advantageous in terms of overall stability. Er<sup>3+</sup>-ions have been used extensively for

both in-fiber and planar dielectric waveguide optical amplifiers.<sup>18</sup> In terms of amplification of SPP signals, the gain provided by Er<sup>3+</sup>-doped materials is insufficient to achieve lossless SPP propagation ( $\text{Im}(k_{\text{SPP}}) = 0$ ), which requires gain corresponding to  $\text{Im}(\epsilon) \approx 3.1 \times 10^{-3}$  ( $44 \text{ cm}^{-1}$ ) at a wavelength of 1550 nm in the case of planar glass–Au interface. Nevertheless, in applications where only partial loss compensation is sufficient, a standard photonic material platform may be advantageous. Again, as in the case of all-optical plasmonic-based modulation, no integratable amplification geometry has yet been demonstrated; usually the pump light is provided out of plane with respect to the active plasmonic structure.

In this Letter we demonstrate suppressed absorption and stimulated emission of SPP signals using copropagating signal and pump SPP waves. The coherent interaction of these waves, mediated by the gain medium, is shown to facilitate all-plasmonic modulation of the SPP signals. The theoretical description of all-plasmonic amplification has also been developed.

The idea for SPP modulation realized here is the following (Figure 1). A control SPP wave, resonantly absorbed by the  $^4I_{15/2} \rightarrow ^4I_{11/2}$  transition, after multiphonon relaxation of the electron to the  $^4I_{13/2}$  level, provides inverse population of the  $^4I_{15/2} \rightarrow ^4I_{13/2}$  transition, which is resonant for a signal SPP wave (see an inset to Figure 1). This suppresses absorption of the signal SPP and leads to stimulated emission of SPPs at this wavelength. Thus, changing the intensity of the control SPP wave therefore determines the transmitted SPP signal leading to the realization of all-plasmonic modulation.

We have used an Er<sup>3+</sup>-ion doped (3 wt % concentration) aluminophosphate glass as a substrate for a 100 nm Au film. The Er<sup>3+</sup>-doped glass is luminescent at around  $\lambda_s = 1550 \text{ nm}$

**Received:** January 22, 2011

**Revised:** March 23, 2011

**Published:** May 04, 2011

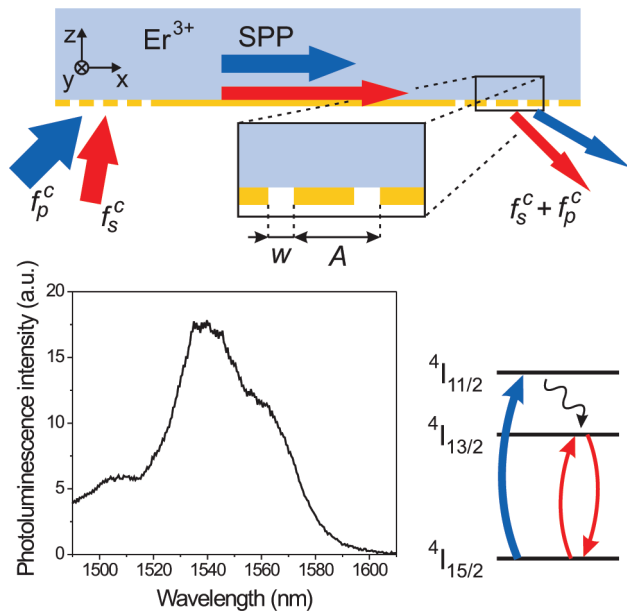


**Figure 1.** Schematic of the experiment for the investigations of SPP stimulated emission and SPP–SPP modulation. The graph shows photoluminescence spectrum of the  $\text{Er}^{3+}$ -doped glass under the excitation with 980 nm wavelength light. The inset represents the diagram of optically active states of an  $\text{Er}^{3+}$ -ion.

(Figure 1), excited as in conventional telecom applications using a  $\lambda_p = 980$  nm wavelength pump. Several pairs of slit gratings were FIB-milled allowing coupling of both signal (at wavelength  $\lambda_s$ ) and control (at the wavelength  $\lambda_p$ ) light into SPP waves propagating on the Au/substrate interface (Figures 1 and 2a, left grating) as well as SPP out-coupling back to light (right grating). For in-coupling gratings having slit width  $w = 100$  nm and period  $A = 1160$  nm, the coupling occurs at  $11^\circ$  and  $45^\circ$  angles of incidence, for signal and pump wavelengths, respectively. The opposite grating (100 nm width and 1990 nm period) allows the out-coupling of the SPP signal reached the grating into photons at an angle of  $48^\circ$ . The distance between the gratings in each pair was varied from 25 to  $250 \mu\text{m}$ .

Initially, the optical properties of both the in-coupling and out-coupling gratings were determined using angle-resolved light transmission measurements. This enables the coupling of both signal and control light to be validated and optimized. The minima of the dispersions shown in Figure 2b correspond to photon coupling to SPP modes on the glass/Au and Air/Au interfaces. The experimental results are in very good agreement with a theoretical model, based on the wave vector matching relation  $k_{\text{SPP}} = k \sin(\varphi) + n(2\pi/A)$ , where  $k$  and  $k_{\text{SPP}}$  are wave vectors of light in free space and SPP wave on a smooth interface, respectively,  $\varphi$  is the angle of incidence,  $A$  is a grating period, and  $n$  is the coupling order. This setup also enable verification of the coupling of the  $\text{Er}^{3+}$ -ion emission into SPP modes on the glass/Au interface.

The experimental setup for SPP–SPP modulation is presented in Figure 1. The signal beam ( $\lambda_s = 1550$  nm) was passed through a polarizer to ensure  $p$ -polarization and was then focused onto the in-coupling grating using a long working distance objective lens. The position of the spot was monitored using the CCD camera. Another IR objective was used to collect the signal from the out-coupling grating. The detection area was

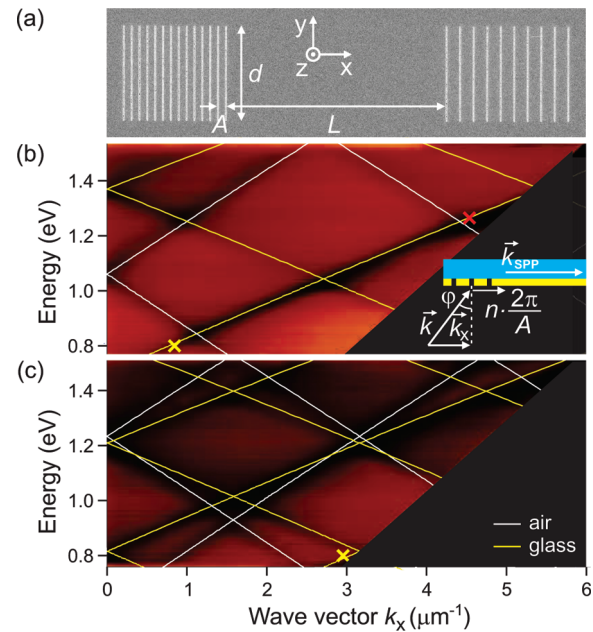


**Figure 2.** (a) SEM image of in-coupling/out-coupling grating pair. (b) Dispersion of the Bragg-scattered SPP modes measured for in-coupling (b) and out-coupling (c) gratings. The dispersion of SPP modes on the smooth gold/air and gold/glass interfaces are presented with white and yellow lines, respectively. The point in the dispersion corresponding to the signal SPP wave coupling and decoupling are marked with the yellow crosses, the point corresponding to the pump SPP wave coupling is marked with a red cross. The vector diagram in (b) describes the mechanism of light-SPP coupling facilitated by a grating.

spatially selected from the image plane using a multimode  $50 \mu\text{m}$  core optical fiber. The particular position of the detection area was adjusted by reversing the light propagation by coupling light into the fiber from the opposite side and monitoring the resulting spot at the sample surface with a camera attached to the objective. Thus, only the light decoupled from the out-coupling grating was collected in the experiment. The collected light was measured using an InGaAs photoreceiver equipped with a long-pass filter to exclude the pump light. The propagation length for signal SPPs at the Au/ $\text{Er}^{3+}$ -glass interface was estimated as  $L_{\text{prop}}^s = 91 \pm 11 \mu\text{m}$  by measuring the output signal for gratings with various separations (see the inset in Figure 3a), which is in a good agreement with the theoretical value of  $94 \mu\text{m}$ . The pump light ( $\lambda_p = 980$  nm) was focused at the in-coupling grating using a metal-coated tapered fiber. For the pump SPP, the propagation length was calculated to be  $L_{\text{prop}}^p = 25 \mu\text{m}$ .

To first approximation, an analytical treatment of all-plasmonic amplification can be achieved using the rate equations for the light-like waves and neglecting the influence of a metal interface on the radiative properties of the emitters. The SPP waves are described as surface photonic waves having a field decay in the direction perpendicular to the metal plane ( $z$ -axis, see the coordinate axis diagrams in Figures 1 and 2a) and internal (Ohmic) losses in the propagation direction ( $x$ -axis). The amplification of the signal intensity  $I_s$  can then be described by the differential equation

$$\frac{dI_s(x)e^{-z/a_s}}{dx} = \left( -\frac{1}{L_{\text{prop}}^p} + \alpha(x, z) \right) I_s(x)e^{-z/a_s} \quad (1)$$

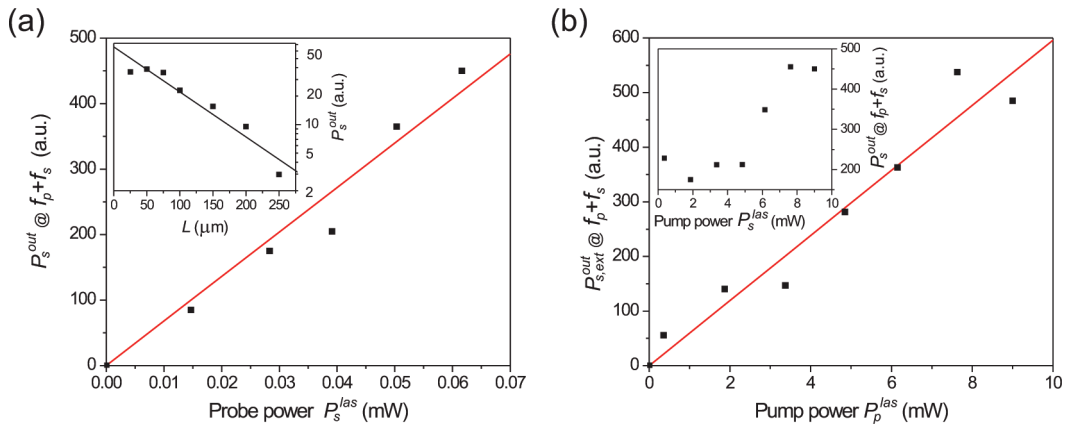


**Figure 3.** Dependences of the SPP–SPP modulation signal  $P_{s,\text{ext}}^{\text{out}}$  on (a) signal laser power  $P_s^{\text{las}}$  and (b) pump laser power  $P_p^{\text{las}}$ . The inset to (a) represents the power of the signal SPP wave (pump is off) on the distance between the in-coupling and out-coupling gratings. The inset to (b) shows the measurements for modulation dependence  $P_s^{\text{out}}$  with a parasitic signal.

where

$$\alpha(x, z) = N \frac{I_p(x, z) \tau \sigma_p \sigma_e - \sigma_a \hbar \omega_p}{\hbar \omega_p + I_p(x, z) \tau \sigma_p} \approx -N \sigma_a + N \frac{\tau \sigma_p}{\hbar \omega_p} (\sigma_e + \sigma_a) I_p(x, z) \quad (2)$$

is the small gain coefficient in small pump approximation  $[(\tau \sigma_p / \hbar \omega_p) I_p \ll 1]$ , the system is far from saturation<sup>19</sup> and

$$I_p(x, z) = I_p^0 e^{-x/L_{\text{prop}}^p} e^{-z/a_p} \quad (3)$$

is the intensity of the pump SPP wave ( $\text{W}/\text{m}^2$ ), where  $I_p^0$  is the intensity at the interface just after the in-coupling grating. Here  $\hbar \omega_p$  is the pump photon energy,  $\sigma_a = 6 \times 10^{-21} \text{ cm}^2$  and  $\sigma_e = 2.6 \times 10^{-21} \text{ cm}^2$  are the absorption and emission cross sections for the signal,  $\sigma_p = 14 \times 10^{-21} \text{ cm}^2$  is the absorption cross-section for the pump,  $\tau = 7.5 \text{ ms}$  is the  $^4I_{13/2}$  state lifetime, and  $N$  is the density of  $\text{Er}^{3+}$ -ions.  $a_s = 606 \text{ nm}$  and  $a_p = 218 \text{ nm}$  are the exponential intensity decay lengths in the direction perpendicular to the metal plane for the signal and pump SPP waves, respectively.

Integrating both sides of equation eq 1 over  $y$  and  $z$ , the equation for the signal SPP power  $P_s$  can be derived as

$$\frac{dP_s(x)}{dx} = \left[ -\beta + \frac{\gamma K}{d} e^{-x/L_{\text{prop}}^p} P_p^0 \right] P_s(x) \quad (4)$$

where  $P_p^0$  is the SPP pump power just after the in-coupling grating

$$\beta = \frac{1}{L_{\text{prop}}^s} + N \sigma_a, \quad \gamma = N \frac{\tau \sigma_p}{\hbar \omega_p} (\sigma_e + \sigma_p) \quad (5)$$

$$K = \frac{\int_0^\infty e^{-z/a_s} e^{-z/a_p} dz}{\int_0^\infty e^{-z/a_s} dz \int_0^\infty e^{-z/a_p} dz} = \frac{1}{a_s + a_p} \quad (6)$$

and  $d$  is the width of the coupling grating (see Figure 2a). Solving eq 4 and representing the solution for the signal SPP

power  $P_s$  at the position of the outcoupling grating ( $x = L$ ) we have

$$P_s(L) = P_s^0 e^{-\beta L} \exp \left[ \gamma K L_{\text{prop}}^p \left( 1 - e^{-L/L_{\text{prop}}^p} \right) \frac{P_p^0}{d} \right] \approx B P_s^0 (1 + \Gamma P_p^0) \quad (7)$$

Here,  $P_s^0$  is the SPP probe power just after the in-coupling grating, the notations  $B$  and  $\Gamma$  are introduced for brevity,  $\Gamma P_p^0$  is therefore the possible modulation depth. As one can see from eqs 5–7, the relative modulation is larger for larger distances, though the overall signal is smaller. This can be expected, since the signal SPP wave is actively modulated over a longer path, while its total magnitude experiences higher attenuation due to Ohmic losses and resonant absorption. One may also note that the modulation also increases with the pump SPP propagation length  $L_{\text{prop}}^p$ . This is also as expected, because at each point along  $x$  there will be an increase in gain.

More importantly, the amplification and modulation of the signal SPP is directly proportional to the overlap between the signal and pump profiles, expressed by the coefficient  $K$  (eq 6). Careful calculation of  $K$  in the case of an SPP pump and an optical pump from the top reveals the overlaps to be of the same order. But here the unique ability of SPPs to localize the field in nanoscale dimensions comes into play; with the same pump power in both cases, the local intensity of the SPP pump will be much higher than the intensity of an off-plane optical pump. Thus, calculated for  $\text{Er}^{3+}$  parameters and for a grating separation of  $L = 20 \mu\text{m}$ , the all-plasmonic approach provides more than 10 times more efficient gain and therefore  $\sim 10$  times higher modulation depth compared to standard out-off plane pumping.

In the experiment, in order to ensure that the SPP signal modulation originates from the coherent interaction of the control and signal beam, a double-modulation lock-in detection scheme was used ensuring that the detected signal is present only when both control and signal SPPs interact with  $\text{Er}^{3+}$ -ion at the same time.<sup>20</sup> The signal beam was mechanically chopped with frequency  $f_s$ . The control light was electronically modulated at the frequency  $f_p$  by the laser-diode controller driven by the signal provided by the chopper controller. The signal detected from the out-coupled signal SPPs was sent to a lock-in amplifier having a reference signal at the sum

frequency  $f_s + f_p$ . Using eq 7, the main harmonics of the signal detected for the grating separation  $L$  can be derived as

$$\begin{aligned}
 P_s(L) &= BP_s^0 \sin(2\pi f_s^c t + \theta_s) [1 + \Gamma P_p^0 \sin(2\pi f_p^c t + \theta_p)] \\
 &= \frac{1}{2} B \Gamma P_s^0 P_p^0 \cos(2\pi (f_s^c + f_p^c) t + \theta_s + \theta_p) \\
 &\quad + P_s^* (f_s^c, f_s^c - f_p^c)
 \end{aligned} \quad (8)$$

where  $\theta_s$  and  $\theta_p$  are the relevant phase delays. Thus, the signal  $1/2 \cdot B \Gamma P_s^0 P_p^0$  detected at the frequency  $f_s + f_p$  is proportional to the modulation  $\Gamma P_p^0$ .

The dependence of the modulated signal on the signal and control light power are presented in Figure 3. The modulation is proportional to the signal and pump laser powers, as expected in the small gain regime (eq 8). By eliminating a parasitic signal (with known phase and magnitude, detected at zero pump power) using a standard formula for subtraction of harmonic oscillations, the component related to the all-plasmonic modulation was recovered (Figure 3b). The resultant dependence on the pump intensity is in agreement with the theoretical predictions of eq 8.

Lightlike amplification theory (eq 2) in many cases is a good first approximation for the case of SPP waves. However, under careful treatment some modifications, representing features specific to SPP wave amplification, must be made.<sup>12,13</sup> The excited lifetime of the emitter is decreased when it is placed in the vicinity of a metal surface. This process can be well approximated by the model of an emitting dipole in the field of its mirror image produced by the metal surface.<sup>21</sup> Applying this to the case of  $\text{Er}^{3+}$ , modeling shows that it can lead to not more than a 20% gain decrease due to the reduction in the spontaneous emission lifetime, depending on the amplification regime.

In conclusion, we have experimentally demonstrated all-plasmonic modulation of an SPP wave at the  $\text{Er}^{3+}$ -doped glass interface using a copropagating pump SPP wave. The modulation is due to suppressed absorption and stimulated emission of a signal SPP wave. A detailed theory accounting for the all-plasmonic nature of signal amplification has been developed to explain the experimental results. We found that the copropagating all-plasmonic approach provided more than 10 times more efficient stimulated emission and therefore  $\sim 10$  times higher modulation depth compared to standard out-of-plane pumping.

The advantages of SPP–SPP modulation demonstrated here on the example of  $\text{Er}^{3+}$ -based active material can be extended towards other gain materials, such as semiconductor quantum dots, polymers, and dye molecules, which can provide faster modulation speed, limited by the stimulated emission rate in the low-gain regime. It should be noted that both stimulated and spontaneous emission rates can be controlled in appropriately designed plasmonic waveguides, for example, metal–insulator–metal or channel waveguides,<sup>22</sup> which provide control over the density of the electromagnetic states and thus electromagnetic field enhancement. This opens a much wider choice of active materials where lifetime at the appropriate wavelength can be selected in the required range to provide the best, for a given application, compromise between the gain and radiation lifetime in the evanescent pump regime.

It should be also noted, that since the modulation depth in the proposed low-gain approach decreases when the length of the active region becomes much smaller than the pump SPP

propagation length  $L_{\text{prop}}^p$  (eq 7), there is a compromise between the achievable modulation depth and the size of the device. To avoid this restriction on the device size and achieve integration in nanophotonic circuitry, one can employ the principle described above within, for example, a plasmonic waveguide ring resonator.<sup>22,23</sup> In the waveguide-based configuration, the plasmonic waveguide that is single mode for the signal wavelength will also support the guiding of the shorter wavelength pump light. The size of such resonators is in the 100–1000 nm range in different realizations, thus indeed providing an integratable element with a sufficient interaction length between pump and signal SPPs needed for efficient modulation.

## AUTHOR INFORMATION

### Corresponding Author

\*E-mail: alexey.krasavin@kcl.ac.uk.

### Present Addresses

<sup>†</sup>Université de Lyon, Institut des Nanotechnologies de Lyon, F-69134 Cedex, France.

<sup>‡</sup>Seagate Technology, 1 Disc Drive, Derry BT48 0BF, U.K.

## ACKNOWLEDGMENT

This work was supported in part by EPSRC (U.K.) and EC FP6 STREP PLASMOCOM. The authors are grateful to D. O'Connor for his assistance in data analysis.

## REFERENCES

- (1) Zayats, A. V.; Smolyaninov, I. I.; Maradudin, A. A. *Phys. Rep.* **2005**, *408*, 131.
- (2) Wurtz, G. A.; Zayats, A. V. *Laser Photonics Rev.* **2008**, *2*, 125.
- (3) Krasavin, A. V.; Zheludev, N. I. *Appl. Phys. Lett.* **2004**, *84*, 1416.
- (4) Pacifici, D.; Lezec, H. J.; Atwater, H. A. *Nat. Photonics* **2007**, *1*, 402.
- (5) Pala, R. A.; Shimizu, K. T.; Melosh, N. A.; Brongersma, M. L. *Nano Lett.* **2008**, *8*, 1506.
- (6) Randhawa, S.; Gonzalez, M. U.; Renger, J.; Enoch, S.; Quidant, R. *Opt. Express* **2010**, *18*, 14496.
- (7) Krasavin, A. V.; Zayats, A. V. *Phys. Rev. B* **2008**, *78*, 045425.
- (8) Krasavin, A. V.; Zayats, A. V. *Opt. Commun.* **2010**, *283*, 1581.
- (9) Nezhad, M. P.; Tetz, K.; Feinman, Y. *Opt. Express* **2004**, *12*, 4072.
- (10) Marini, A.; Gorbach, A. V.; Skryabin, D. V.; Zayats, A. V. *Opt. Lett.* **2009**, *34*, 2864.
- (11) Seidel, J.; Grafstrom, S.; Eng, L. *Phys. Rev. Lett.* **2005**, *94*, 177401.
- (12) De Leon, I.; Berini, P. *Phys. Rev. B* **2008**, *78*, 161401(R).
- (13) De Leon, I.; Berini, P. *Nat. Photonics* **2010**, *4*, 382.
- (14) Gather, M. C.; Meerholz, K.; Danz, N.; Leosson, K. *Nat. Photonics* **2010**, *4*, 457.
- (15) Ambati, M.; Nam, S. H.; Ulin-Avila, E.; Genov, D. A.; Bartal, G.; Zhang, X. *Nano Lett.* **2008**, *8*, 3998.
- (16) Granddier, J.; Colas des Francs, G.; Massenet, S.; Bouhelier, A.; Markey, L.; Weeber, J.-C.; Finot, C.; Dereux, A. *Nano Lett.* **2009**, *9*, 2935.
- (17) Bolger, P. M.; Dickson, W.; Krasavin, A. V.; Liebscher, L.; Hickey, S. G.; Skryabin, D. V.; Zayats, A. V. *Opt. Lett.* **2010**, *35*, 1197.
- (18) *Optical fiber amplifiers: materials, devices and applications*; Sudo, S., Ed.; Artech House Publishers: London, 1997.
- (19) Nair, L. G. *Prog. Quantum Electron* **1982**, *7*, 153.
- (20) Bolger, P.; Vo, T. P.; Krasavin, A.; Dickson, W.; Zayats, A. *4th International conference on Surface Plasmon Photonics* (Amsterdam, The Netherlands, 2009), P-MON-020-B.

(21) Hartman, R. L.; Cohen, S. M.; Leung, P. T. *J. Chem. Phys.* **1999**, *110*, 2189.

(22) Vesseur, E. J. R.; de Abajo, F. J. G.; Polman, A. *Phys. Rev. B* **2010**, *82*, 165419.

(23) Krasavin, A. V.; Zayats, A. V. *Appl. Phys. Lett.* **2010**, *97*, 041107.

#### ■ NOTE ADDED AFTER ASAP PUBLICATION

Equation 7 was incorrect in the version of this paper published May 4, 2011. The correct version published May 6, 2011.